Discretisation and Solver Methods for a Model for Solid-Gas-Phase of a Crystal Growth Apparatus.

Jürgen Geiser

Humboldt-Universität zu Berlin, Department of Mathematics, Unter den Linden 6, D-10099 Berlin, Germany

Abstract

We present discretisation and solver methods for a model for a solid-gas phase of a crystal growth apparatus. The model-equations are coupled Eulerian- and Heat-transfer-equations with flux-boundary conditions. For more detailed discussion we consider simpler equations and present time- and space-decomposition methods as a solver methods to decouple the multi-physics processes. We present the error-analysis for the discretisation methods and solver methods. Numerical experiments are done for the eulerrian- and heat-transfer-equation with decomposition methods. We present a real-life application of a crystal growth apparatus, based on the underlying stationary heat conduction. Finally we discuss the further works in the error-analysis and the application to a more complex model of crystal growth.

Key words: decomposition methods, finite volume discretisation, error-analysis, heat-eqaution, crystal growth
PACS: 02.60.Cb, 02.60.-x, 44.05.+e, 47.10.ab, 47.11.Df, 47.11.St, 47.27.te

1 Introduction

Modeling and numerical simulation of solid-gas phase in complex apparatus have become powerful tools in aiding the design and optimization of numerous industrial processes such as crystal growth, e.g. by the physical vapor transport (PVT) method Klein et al. [19]. Because of the complex processes a carefully study is important to design correct the numerical simulations, Parashar et al. [29]. Based on this background the combination of discretisation and solver methods is an important task. We propose the decompostion methods of breaking down complicate multiphysics in simpler physics. The time-decomposition methods are based on Operator-Splitting methods and

their extended versions with more stabilised behaviour, see Farago & Geiser [12]. With this methods a useful decoupling of the time-scales are possible and the solvers could be concentrate on the different time-scales. Further the space-decomposition methods are based on the Schwarz wave form relaxation methods and their accurate error-estimates, see Daoud & Geiser [8]. The methods decouple into domains with the same equation-parameters, therefore effective spactial discretisation and solver methods are appliable.

The paper is organized as follows: The mathematical model is stated in Section 2, the space-discretisation methods are done with finite volume discretization and described in Section 3, followed by the time-discretisation methods as Runge-Kutta- and BDF-methods presented in Section 4. The time-decomposition methods are introduced as Operator-Splitting method with extended variations in Section 5. In Section 6, we describe the space-decompostion methods in the sense of Schwarz wave form relaxation methods and describe the analytical error-estimates. In Section 7 we describe the numerical methods in which we verify our decomposition methods and simulate a realistic crystal-growth apparatus.

2 Mathematical model

The motivation for this study comes from the technical demand to simulate a crystal growth apparatus for SiC single crystals. The single crystals are used as a high-valued and expensive material for optoelectronics and electronics, see Müller et al. [27]. The silicon carbide (SiC) bulk single crystal are produced by a growth process through physical vapor transport (PVT), called modified Lely-method. The modeling for the thermal processes within the growth apparatus is done in Klein & Philip [20] and Philip [30]. The underlying equations of the model are given as follows:

a.) In this work, we assume that the temperature evolution inside the gas region Ω_{g} can be approximated by considering the gas as pure argon. The reduced heat equation is

$$\rho_{\mathrm{g}} \partial_t U_{\mathrm{g}} \; - \; \nabla \cdot (\kappa_{\mathrm{g}} \nabla T) = 0, \tag{1}$$

$$U_{\mathrm{g}} = z_{\mathrm{Ar}} \, R_{\mathrm{Ar}} \, T, \tag{2}$$

where T is the temperature, t is the time, and U_{g} is the internal energy of the argon gas. The parameters are given as ρ_{g} being the density of the argon gas, κ_{g} being the thermal conductivity, z_{Ar} being the configuration number, and R_{Ar} being the gas constant for argon.

b.) The temperature evolution inside the region of solid materials Ω_{s}, e.g. in-

side the silicon carbide crystal, silicon carbide powder, graphite, and graphite insulation, is described by the heat equation

$$\rho_{\mathrm{s}}\, \partial_t U_{\mathrm{s}} \; - \; \nabla \cdot (\kappa_{\mathrm{s}} \nabla T) = f, \tag{3}$$

$$U_{\mathrm{s}} = \int_0^T \; c_{\mathrm{s}}(S)\, dS, \tag{4}$$

where ρ_{s} is the density of the solid material, U_{s} is the internal energy, κ_{s} is the thermal conductivity, and c_{s} is the specific heat.

The equations hold in the domains of the respective materials and are coupled by interface conditions, e.g. requiring the continuity for the temperature and for the normal components of the heat flux on the interfaces between opaque solid materials. On the boundary of the gas domain, i.e. on the interface between the solid material and the gas domain, we consider the interface condition

$$\kappa_{\mathrm{g}}\; \nabla T \cdot \mathbf{n}_{\mathrm{g}} + R - J = \kappa_{\mathrm{s}}\; \nabla T \cdot \mathbf{n}_{\mathrm{g}}, \tag{5}$$

where $\mathbf{n}_{\mathrm{g}}$ is the normal vector of the gas domain, R is the radiosity, and J is the irradiosity. The irradiosity is determined by integrating R along the whole boundary of the gas domain, see Klein & Philip [20]. Moreover, we have

$$R = E + J_{\mathrm{ref}}, \tag{6}$$

$$E = \sigma\, \epsilon\, T^4 \quad \text{(Stefan-Boltzmann equation)}, \tag{7}$$

$$J_{\mathrm{ref}} = (1 - \epsilon)\, J, \tag{8}$$

where E is the radiation, J_{ref} is the reflexed radiation, ϵ is the emissivity, and σ is the Boltzmann radiation constant.

In the next section, we focus on decoupling the complicate process in simpler processes. We discretise and solve the simpler equations by more accurate methods with embedded analytical solutions, see Geiser [15], Geiser [16].

3 Space discretization

In the space discretisation methods we discuss the finite volume methods as conservation preserved methods for the balance-equations.

The Finite Volume methods are robust discretisation methods for conservative problems. We apply the discretisation because of the simple modifications for the different material behaviour, for instance the anisotropic thermal conductivity is important.

There exists standard techniques including the finite element method Ciarlet et al. [7] (used in Dupret et al. [9]) and the finite volume method Eymard et al. [10] to treat such problems. The extension of such standard methods to materials with anisotropic thermal conductivity can be straightforward for simple geometries (e.g. if the geometry admits a discretization into a structured grid of rectangles or parallelepipeds). However, the treatment of anisotropic materials within complex geometries as they are typical in industrial applications are necessary are much more involved. To the authors' knowledge, even for two-dimensional domains, all the methods previously described in the literature are restricted to simple classes of domains, need to be adapted to fit the type of anisotropy, or show instabilities for strongly anisotropic materials (see, e.g., Aavatsmark et al. [1, 2], Braianov & Volkov [5], Faille [11] and [10, Sec. 11]).

We use a constrained Delaunay triangulation to discretize polyhedral domains, followed by a Voronoï construction to define finite volumes, is a well-known procedure (see [FL01, Sec. 3.2] and references therein). Here, we briefly review some definitions and properties that are subsequently used in the formulation of the finite volume scheme for the anisotropic case.

Following [FL01, Sec. 3.2], an admissible discretization of material domain Ω_m, $m \in M$, consists of a finite family $\Sigma_m := (\sigma_{m,i})_{i \in I_m}$ of subsets of Ω_m satisfying a number of assumptions, subsequently denoted by (DA-$*$).

Notation 1 *For $d \in \{1, 2\}$, let λ_d denote d-dimensional Lebesgue measure.*

(DA-1) For each $m \in M$, $\Sigma_m = (\sigma_{m,i})_{i \in I_m}$ forms a finite conforming triangulation of Ω_m. In particular, for each $i \in I_m$, $\sigma_{m,i}$ is an open triangle. Moreover, letting $I := \bigcup_{m \in M} I_m$, $\Sigma := (\sigma_i)_{i \in I}$ forms a conforming triangulation of Ω.

(DA-2) For each $m \in M$, the triangulation $\Sigma_m = (\sigma_{m,i})_{i \in I_m}$ respects Γ_{Dir} and Γ_{Rob} in the sense that, for each $i \in I_m$, either $\lambda_1(\Gamma_{\mathrm{Dir}} \cap \partial\sigma_{m,i}) = 0$ or $\lambda_1(\Gamma_{\mathrm{Rob}} \cap \partial\sigma_{m,i}) = 0$.

For each $\sigma_{m,i}$, let $V(\sigma_{m,i}) = \left\{ v_{i,j}^m : j \in \{1, 2, 3\} \right\}$ denote the set of vertices of $\sigma_{m,i}$, and let $V := \bigcup_{m \in M,\, i \in I_m} V(\sigma_{m,i})$ be the set of all vertices in the triangulation. One can then define the control volumes as the Voronoï cells with

respect to the vertices. Using $\|\cdot\|_2$ to denote Euclidean distance, define

$$\text{for all } v \in V\colon \omega_v := \Big\{x \in \Omega : \|x - v\|_2 < \|x - z\|_2 \text{ for each } z \in V \setminus \{v\}\Big\},$$
$$\text{for all } m \in M\colon \omega_{m,v} := \omega_v \cap \Omega_m, \quad V_m := \{z \in V : \omega_{m,z} \neq \emptyset\}.$$

Letting $\mathcal{T} := (\omega_v)_{v\in V}$, $\mathcal{T}_m := (\omega_{m,v})_{v\in V_m}$, $m \in M$, $\mathcal{T}$ forms a partition of Ω, and $\mathcal{T}_m$ forms a partition of Ω_m.

Remark 2 *Since $\mathcal{T}$ is a Voronoï discretization, each intersection $\partial\omega_v \cap \partial\omega_z$, $(v,z) \in V^2$, $v \neq z$, is contained in the set $\{x \in \Omega : \|v - x\|_2 = \|z - x\|_2\}$. In particular, $\frac{z-v}{\|z-v\|_2} = \mathbf{n}_{\omega_v}\restriction_{\partial_{\mathrm{reg}}\omega_v \cap \partial_{\mathrm{reg}}\omega_z}$, where ∂_{reg} denotes the regular boundary of a polyhedral set, i.e. the points of the boundary, where a unique outer unit normal vector exists, $\partial_{\mathrm{reg}}\emptyset := \emptyset$; and $\mathbf{n}_{\omega_v}\restriction_{\partial_{\mathrm{reg}}\omega_v \cap \partial_{\mathrm{reg}}\omega_z}$ is the outer unit normal to ω_v restricted to the face $\partial_{\mathrm{reg}}\omega_v \cap \partial_{\mathrm{reg}}\omega_z$ (see Fig. 1).*

Notation 3 *If $A \subseteq \mathbb{R}^2$, then* conv A *denotes the convex hull of A. For each pair of points $(x,y) \in \mathbb{R}^2 \times \mathbb{R}^2$, let $[x,y] := \mathrm{conv}\{x,y\}$ denote the line segment between x and y.*

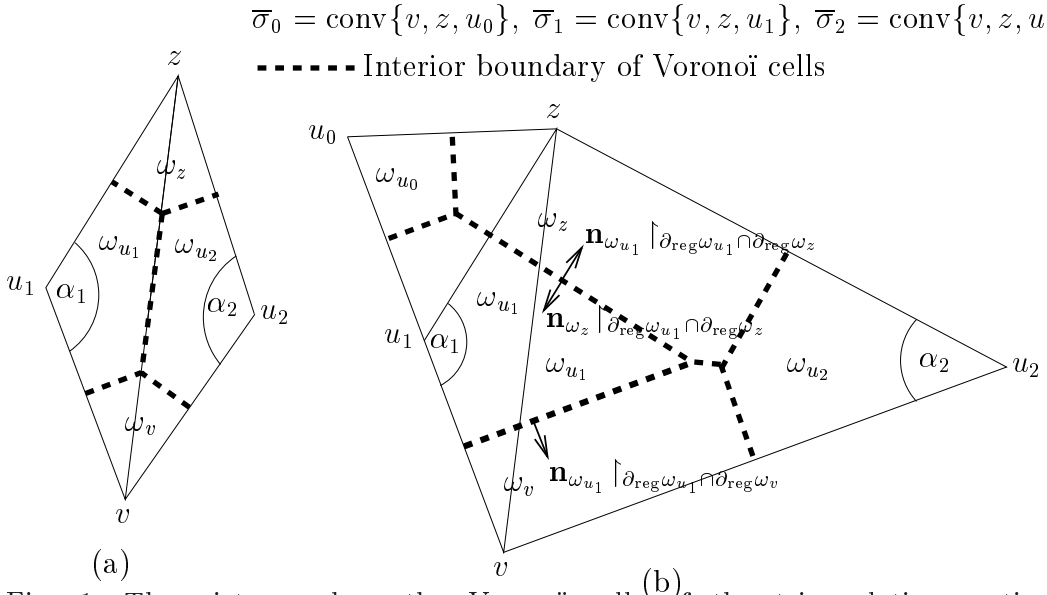

Fig. 1. The pictures show the Voronoï cells of the triangulation vertices u_0, u_1, u_2, v, z. In (a), the triangulation violates the constrained Delaunay property ($\alpha_1 + \alpha_2 > \pi$, cf. (DA-1) and Rem. 4); in (b) the constrained Delaunay property is satisfied if, and only if, the edge $[v,z]$ is not a material interface ($\pi/2 < \alpha_1$, $\alpha_1 + \alpha_2 < \pi$).

(DA-1) For each $m \in M$, the triangulation Σ_m has the constrained Delaunay property: If $\tilde{V}_m := \bigcup_{i\in I_m} V(\sigma_{m,i})$; then, for each $(v,z) \in \tilde{V}_m^2$ such that $v \neq z$, the following conditions (a) and (b) are satisfied:
  (a) If the boundaries of the Voronoï cells corresponding to v and z have a one-dimensional intersection, i.e. if $\lambda_1(\partial\omega_{m,v} \cap \partial\omega_{m,z}) \neq 0$, then $[v,z]$ is an edge of at least one $\sigma \in \Sigma_m$.

(b) If $[v, z]$ is an edge of at least one $\sigma \in \Sigma_m$, then the boundaries of the corresponding Voronoï cells have a nonempty intersection, i.e. $\partial\omega_{m,v} \cap \partial\omega_{m,z} \neq \emptyset$.

Also see Fig. 1, Rem. 4, and [FL01, Sec. 3.2].

Remark 4 *Due to the two-dimensional setting,* (DA-1) *can be expressed equivalently in terms of the angles in the triangulation: For each $m \in M$, if γ is an interior edge of the triangulation Σ_m, and α and β are the angles opposite to γ, then $\alpha + \beta \leq \pi$. If $\gamma \subseteq \partial\Omega_m$ is a boundary edge of Σ_m, and α is the angle opposite γ, then $\alpha \leq \pi/2$.*

The following Rem. 5 allows the incorporation of the interface condition (78) into the finite volume scheme.

Remark 5 *Using Rem. 2, it is not hard to show that* (DA-1) *and* (DA-1) *imply the following assertions* (a) *and* (b)*:*

(a) For each $m \in M$, the set V_m defined in (9a) *is identical to the set $\tilde{V}_m$ defined in* (DA-1)*.*

(b) Let Γ be a one-dimensional material interface: $\Gamma = \partial\Omega_m \cap \partial\Omega_{\tilde{m}}$, $\lambda_1(\Gamma) \neq 0$. For each $v \in V$, if some $\overline{\omega}_v$ has a one-dimensional intersection with the interface Γ, then it lies on both sides of the intersection; in other words, $\partial_{\mathrm{reg}}\omega_{m,v} \cap \Gamma = \partial_{\mathrm{reg}}\omega_{\tilde{m},v} \cap \Gamma$, in particular, $\lambda_1(\partial\omega_{m,v} \cap \Gamma) \neq 0$ if, and only if $\lambda_1(\partial\omega_{\tilde{m},v} \cap \Gamma) \neq 0$. However, Fig. 1(a) shows that this can generally not be expected in cases where the constrained Delaunay property is violated: If the edge $[v, w] =: \Gamma$ constitutes a material interface, then both $\overline{\omega}_{u_1}$ and $\overline{\omega}_{u_2}$ have one-dimensional intersections with Γ, but lie on just one side of Γ.

Integrating (76) over $\omega_{m,v}$ and applying the Gauss-Green integration theorem yields

$$-\int_{\partial\omega_{m,v}} (K_m(\theta)\,\nabla\theta) \bullet \mathbf{n}_{\omega_{m,v}} = \int_{\omega_{m,v}} f_m, \tag{10}$$

where $\mathbf{n}_{\omega_{m,v}}$ denotes the outer unit normal vector to $\omega_{m,v}$.

4 Time-discretisation methods

For the time-discretization of the spatial discretised equation we apply Runge-Kutta methods and BDF methods.

For the equation treated with operator-splitting, we propose we propose higher order methods as best fitted methods for each time-scale. A next important class of time-discretisation methods are the IMEX (implicit-explicit) methods

as combination of mixed discretisation methods for a stiff-operators (implicit method) and nonstiff-operators (explicit method).

Based on the iterative methods the start-solution for the first iteration-step is important to obtain higher order results, see section 5. For the next iteration steps the order have to increased till the proposed order of the time-discretization.

The methods are described in the following sections.

4.1 Runge-Kutta method

We use the implicit trapezoidal rule:

$$\begin{array}{c|cc} 0 & & \\ 1 & \frac{1}{2} & \frac{1}{2} \\ \hline & \frac{1}{2} & \frac{1}{2} \end{array} \tag{11}$$

Further more we use the following Gauß Runge-Kutta method :

$$\begin{array}{c|cc} \frac{1}{2}-\frac{\sqrt{3}}{6} & \frac{1}{4} & \frac{1}{4}-\frac{\sqrt{3}}{6} \\ \frac{1}{2}+\frac{\sqrt{3}}{6} & \frac{1}{4}+\frac{\sqrt{3}}{6} & \frac{1}{4} \\ \hline & \frac{1}{2} & \frac{1}{2} \end{array} \tag{12}$$

To use this Runge-Kutta methods with our operator-splitting method we have to take into account that we solve in each iteration step equations of the form $\partial_t u_i = Au_i + b$. Where $b = Bu_{i-1}$ is a discrete function as we only have a discrete solution for u_{i-1}.
For the implicit trapezoidal rule this is no problem, because we do not need the values at any sub-points. Where on the other hand for the Gauß method we need to now the values of b at the sub-points $t_0 + c_1 h$ and $t_0 + c_2 h$ with $c = (\frac{1}{2} - \frac{\sqrt{3}}{6}, \frac{1}{2} + \frac{\sqrt{3}}{6})^T$. Therefor we must interpolate b. To do so we choose the cubic spline functions.
Numerical experiments show that this works properly with non-stiff problems, but worth with stiff-problems.

4.2 BDF method

Because the higher order Gauß Runge-Kutta method combined with cubic spline interpolation does not work properly with stiff problems we use the following BDF method of order 3 which does not need any sub-points and therefor no interpolation is needed.

BDF3

$$1/k(11/6u^{n+2} - 3u^{n+1} + 3/2u^n - 1/3u^{n-1} = A(u^{n+3}) \tag{13}$$

For the prestepping, i.e. to obtain u_1, u_2, we use the above implicit trapezoidal rule.

4.3 Implicit-explicit methods

The implicit-explicit (IMEX) schemes have been widely developed for time integration of spatial discretised partial differential equations of diffusion-convection type. These methods are applied to decouple the implicit and explicit terms. So for example the convection-diffusion equation, one use the explicit part for the convection term and the implicit part for the diffusion. In our application we divide between the stiff and nonstiff term, so we apply the implicit part for the stiff operators and the explicit part for the nonstiff operators.

4.3.1 FS-RK-method

We propose the A-stable FSRK-scheme, see **?**], of first and second order for our applications.
The tableau in the Butcher-form is given as

$$\begin{array}{c|cccc|cccc}
1 & 1 & & & & 0 & & & \\
1 & 1 & 0 & & & 0 & 1 & & \\
\frac{4}{9} & -\frac{88}{45} & 0 & \frac{12}{5} & 0 & 0 & \frac{5}{9} & 0 & \\
\frac{1}{3} & -\frac{407}{75} & 0 & \frac{144}{25} & 0 & 0 & -\frac{31}{15} & 0 & \frac{12}{5} \\
\hline
\text{order1} & 1 & 0 & 0 & 0 & 0 & 1 & 0 & 0 \\
\hline
\text{order2} & \frac{1}{10} & 0 & \frac{9}{10} & 0 & 0 & \frac{1}{4} & 0 & \frac{3}{4}
\end{array} \tag{14}$$

To obtain second order convergence in numerical examples it is important to split the operator in the right way as we will show later.

4.3.2 SBDF-Method

We use the following SBDF method which is a modification of the BDF3 method.
As prestepping method we use again the implicit trapezoidal rule.

$$1/k(11/6u^{n+1} - 3u^n + 3/2u^{n-1} - 1/3u^{n-2}) \tag{15}$$
$$= 3A(u^n) - 3A(u^{n-1}) + A(u^{n-2}) + B(u^{n+1}) \tag{16}$$

Again it is important to split the operator in the right way.

5 Time-Decomposition methods: Operator-Splitting Methods

The operator-splitting methods are used to solve complex models in the geophysical and environmental physics, they are developed and applied in Strang [36] and Verwer & Sportisse [37]. This ideas based in this article are solving simpler equations with respect to receive higher order discretization methods for the remain equations. For this aim we use the operator-splitting method and decouple the equation as follows described.

5.1 Splitting methods of first order for linear equations

First we describe the simplest operator-splitting, which is called β for the following system of ordinary linear differential equations:

$$\partial_t c(t) = A\ c(t)\ +\ B\ c(t)\ , \tag{17}$$

whereby the initial-conditions are $c^n = c(t^n)$. The operators A and B are spatially discretised operators, e.g. they correspond to the discretised in space convection and diffusion operators (matrices). Hence, they can be considered as bounded operators.

The sequential operator-splitting method is introduced as a method which solve the two sub-problems sequentially, where the different sub-problems are connected via the initial conditions. This means that we replace the original problem (17) with the sub-problems

$$\frac{\partial c^*(t)}{\partial t} = Ac^*(t)\ , \quad \text{with } c^*(t^n) = c^n\ , \tag{18}$$
$$\frac{\partial c^{**}(t)}{\partial t} = Bc^{**}(t)\ , \quad \text{with } c^{**}(t^n) = c^*(t^{n+1})\ ,$$

whereby the splitting time-step is defined as $\tau_n = t^{n+1} - t^n$. The approximated split solution is defined as $c^{n+1} = c^{**}(t^{n+1})$.

Clearly, the change of the original problems with the sub-problems usually results some error, called *splitting error*. Obviously, the splitting error of the ß method can be derived as follows (cf. e.g.**?**])

$$\begin{aligned}\rho_n &= \frac{1}{\tau}(\exp(\tau_n(A+B)) - \exp(\tau_n B)\exp(\tau_n A))\ c(t^n) \\ &= \frac{1}{2}\tau_n[A,B]\ c(t^n) + O(\tau^2)\ .\end{aligned} \tag{19}$$

whereby $[A,B] := AB - BA$ is the commutator of A and B. Consequently, the splitting error is $O(\tau_n)$ when the operators A and B do not commute, otherwise the method is exact. Hence, by definition, the ß is called *first order splitting method* .

In the next subsection we present the iterative-splitting method.

5.2 Iterative splitting method

The following algorithm is based on the iteration with fixed splitting discretization step-size τ, namely, on the time interval $[t^n, t^{n+1}]$ we solve the following sub-problems consecutively for $i = 0, 2, \ldots 2m$. (cf. Kanney et al. [18] and Farago & Geiser [12].)

$$\frac{\partial c_i(t)}{\partial t} = Ac_i(t)\ +\ Bc_{i-1}(t), \text{ with } \ c_i(t^n) = c^n \tag{20}$$
and $c_0(t^n) = c^n\ ,\ c_{-1} = 0.0,$
$$\frac{\partial c_{i+1}(t)}{\partial t} = Ac_i(t)\ +\ Bc_{i+1}(t), \tag{21}$$
with $\ c_{i+1}(t^n) = c^n\ ,$

where c^n is the known split approximation at the time level $t = t^n$. The split approximation at the time-level $t = t^{n+1}$ is defined as $c^{n+1} = c_{2m+1}(t^{n+1})$. (Clearly, the function $c_{i+1}(t)$ depends on the interval $[t^n, t^{n+1}]$, too, but, for the sake of simplicity, in our notation we omit the dependence on n.)

In the following we will analyze the convergence and the rate of the convergence of the method (20)–(21) for m tends to infinity for the linear operators $A, B : \mathbf{X} \to \mathbf{X}$ where we assume that these operators and their sum are generators of the C_0 semigroups. We emphasize that these operators aren't necessarily bounded, so, the convergence is examined in general Banach space setting.

Theorem 6 *Let us consider the abstract Cauchy problem in a Banach space* $\mathbf{X}$

$$\begin{aligned} \partial_t c(t) &= Ac(t) + Bc(t), \quad 0 < t \leq T \\ c(0) &= c_0 \end{aligned} \tag{22}$$

where $A, B, A + B : \mathbf{X} \to \mathbf{X}$ *are given linear operators being generators of the* C_0*-semigroup and* $c_0 \in \mathbf{X}$ *is a given element. Then the iteration process (20)–(21) is convergent and the and the rate of the convergence is of second order.*

Remark 7 When A and B are matrices (i.e. (20)–(21) is a system of the ordinary differential equations), for the growth estimation we can use the concept of the logarithmic norm. (See e.g.Hundsdorfer & Verwer [17].) Hence, for many important class of matrices we can prove the validity.

Remark 8 We note that a huge class of important differential operators generate contractive semigroup. This means that for such problems -assuming the exact solvability of the split sub-problems- the iterative splitting method is convergent in second order to the exact solution.

5.3 Weighted Iterative splitting method

We assume an improved iterative splitting method with respect to more stable behavior in the continuous case.

As a first method the unsymmetric weighted iterative splitting method is introduced. The algorithm is based on the iteration with fixed splitting discretization step-size τ. On the time interval $[t^n, t^{n+1}]$ we solve the following sub-problems consecutively for $i = 0, 2, \ldots 2m$.

$$\frac{\partial c_i(t)}{\partial t} = Ac_i(t) \ + \ \omega \, Bc_{i-1}(t), \text{ with } \ c_i(t^n) = c^n \tag{23}$$
and $c_0(t^n) = c^0 \ , \ c_{-1} = 0,$
$$\frac{\partial c_{i+1}(t)}{\partial t} = \omega \, Ac_i(t) \ + \ Bc_{i+1}(t), \tag{24}$$
with $\ c_{i+1}(t^n) = \omega \, c^n + (1-\omega) \, c_i(t^{n+1}) \ ,$

where c^n is the known split approximation at the time level $t = t^n$. The split approximation at the time-level $t = t^{n+1}$ is defined as $c^{n+1} = c_{2m+1}(t^{n+1})$. Our parameter $\omega \in [0, 1]$. For $\omega = 0$ we have the A-B-splitting and for $\omega = 1$ we have the iterative splitting method.

In the same manner the initial conditions of the weighted iterative splitting method are weighted between the sequential splitting and iterative splitting method.

5.4 Stability Theory

In the following we present the stability analysis for the continuous case with commutative operators. First we apply the recursion for the general case and then we concentrate on the commutative case.

5.4.1 Recursion

We study the stability for the linear system (23) and (24). We treat the special case for the initial-values with $c_i(t^n) = c_n$ and $c_{i+1}(t^n) = c_n$ for an overview. The general case $c_{i+1}(t^n) = \omega c_n + (1-\omega)c_i(t^{n+1})$ could be treated in the same manner.

We consider the suitable vector norm $||\cdot||$ on $\mathbb{R}^M$, together with its induced operator norm. The matrix exponential of $Z \in \mathbb{R}^{M\times M}$ is denoted by $\exp(Z)$. We assume that

$$||\exp(\tau \, A) \leq 1|| \ \text{ and } \ ||\exp(\tau \, B) \leq 1|| \ \text{ for all } \ \tau > 0.$$

It can be shown that the system (17) implies $||\exp(\tau \ (A+B))|| \leq 1$ and is itself stable.

For the linear problem (23) and (24) it follows by integration that

$$c_i(t) = \exp((t-t^n)A)c^n + \int_{t^n}^{t} \exp((t-s)A)\ \omega\ Bc_{i-1}(s)\ ds\ , \tag{25}$$

$$c_{i+1}(t) = \exp((t-t^n)B)c^n + \int_{t^n}^{t} \exp((t-s)B)\ \omega\ Ac_{i}(s)\ ds\ . \tag{26}$$

With elimination of c_i we get

$$\begin{aligned} c_{i+1}(t) = \exp((t-t^n)B)c^n\ &+\ \omega\ \int_{t^n}^{t} \exp((t-s)B)\ A\ \exp((s-t^n)A)\ c^n\ ds \\ +\omega^2\ &\int_{s=t^n}^{t}\ \int_{s'=t^n}^{s} \exp((t-s)B)\ A\ \exp((s-s')A)\ B\ c_{i-1}(s')\ ds'\ ds\ . \end{aligned} \tag{27}$$

For the following commuting case we could evaluate the double integral $\int_{s=t^n}^{t}\ \int_{s'=t^n}^{s}$ as $\int_{s'=t^n}^{t}\ \int_{s=s'}^{t}$ and could derive the weighted stability-theory.

5.4.2 Commuting operators

For more transparency of the formula (27) we consider a well-conditioned system of eigenvectors and the eigenvalues λ_1 of A and λ_2 of B instead of the operators A, B themselves. Replacing the operators A and B by λ_1 and λ_2 respectively, we obtain after some calculations

$$\begin{aligned} c_{i+1}(t) = c^n &\frac{1}{\lambda_1-\lambda_2}\left(\omega\lambda_1 \exp((t-t^n)\lambda_1) + ((1-\omega)\lambda_1 - \lambda_2)\exp((t-t^n)\lambda_2)\right) \\ &+ c^n\ \omega^2\ \frac{\lambda_1\lambda_2}{\lambda_1-\lambda_2}\ \int_{s=t^n}^{t} \left(\exp((t-s)\lambda_1)\ -\ \exp((t-s)\lambda_2)\right) ds\ . \end{aligned} \tag{28}$$

Note that this relation is symmetric in λ_1 and λ_2.

5.4.3 $A(\alpha)$-stability

We define $z_k = \tau\lambda_k$, $k = 1, 2$. We start with $c_0(t) = u^n$ and we obtain

$$c_{2m}(t^{n+1}) = S_m(z_1, z_2)\ c^n\ , \tag{29}$$

where S_m is the stability function of the scheme with m-iterations. We use (28) and obtain after some calculations

$$S_1(z_1,z_2) = \omega^2\ c^n\ +\ \frac{\omega\ z_1 + \omega^2\ z_2}{z_1 - z_2}\ \exp(z_1)\ c^n + \frac{(1-\omega-\omega^2)\ z_1 - z_2}{z_1 - z_2}\ \exp(z_2)\ c^n \tag{30}$$

$$\begin{aligned} S_2(z_1,z_2) = {} & \omega^4\ c^n\ +\ \frac{\omega\ z_1 + \omega^4\ z_2}{z_1 - z_2}\ \exp(z_1)\ c^n \\ & + \frac{(1-\omega-\omega^4)\ z_1 - z_2}{z_1 - z_2}\ \exp(z_2)\ c^n \\ & + \frac{\omega^2\ z_1\ z_2}{(z_1 - z_2)^2}\ ((\omega z_1 + \omega^2 z_2)\exp(z_1) \\ & +(-(1-\omega-\omega^2)z_1 + z_2)\exp(z_2))\ c^n \\ & + \frac{\omega^2\ z_1\ z_2}{(z_1 - z_2)^3}\ ((-\omega z_1 - \omega^2 z_2)(\exp(z_1) - \exp(z_2)) \\ & +((1-\omega-\omega^2)z_1 - z_2)(\exp(z_1) - \exp(z_2)))\ c^n \end{aligned} \tag{31}$$

Let us consider the $A(\alpha)$-stability given by the following eigenvalues in a wedge

$W = \{\zeta \in C : |\arg(\zeta) \leq \alpha\}$

For the A-stability we have $|S_m(z_1,z_2)| \leq 1$ whenever $z_1, z_2 \in W_{\pi/2}$.
The stability of the two iterations is given in the following theorem with respect to A and $A(\alpha)$-stability.

Theorem 9 *We have the following stability :*

For S_1 we have the A-stability
$\max_{z_1 \leq 0, z_2 \in W_\alpha} |S_1(z_1,z_2)| \leq 1\ ,\ \forall\ \alpha \in [0,\pi/2]$ *with* $\omega = \frac{1}{\sqrt[4]{3}}$

For S_2 we have the $A(\alpha)$-stability
$\max_{z_1 \leq 0, z_2 \in W_\alpha} |S_2(z_1,z_2)| \leq 1\ ,\ \forall\ \alpha \in [0,\pi/2]$ *with* $\omega \leq \left(\frac{1}{8\ \tan^2(\alpha)+1}\right)^{1/8}$

Proof 10 *We consider a fixed $z_1 = z$, $Re(z) < 0$ and $z_2 \to -\infty$. Then we obtain*

$$S_1(z,\infty) = \omega^2(1 - e^z) \tag{32}$$

and

$$S_2(z,\infty) = \omega^4(1-(1-z)e^z) \tag{33}$$

If $z = x + iy,\ x < 0$ *then :*

1.) For S_1

$$|S_1(z,\infty)|^2 = \omega^4(1 - 2\exp(x)cosy + \exp(2x)) \tag{34}$$

Hence

$$|S_1(z,\infty)| \leq 1 \Leftrightarrow \omega^4 \leq \frac{1}{1 - 2\exp(x)\ \cos y + \exp(2x)} \tag{35}$$

Because of $x < 0$ *and* $y \in \mathbb{R}$ *we could estimate* $-2 \leq 2\exp(x)\ \cos(y)$ *and* $\exp(2x) \geq 0$.
From (35) we obtain $\omega \leq \frac{1}{\sqrt[4]{3}}$.

2.) For S_2

$$\begin{aligned} |S_2(z,\infty)|^2 = &\omega^8\{1 - 2\exp(x)[(1-x)\cos y + y\sin y] \\ &+ \exp(2x)[(1-x)^2 + y^2]\} \end{aligned} \tag{36}$$

after some calculations we could obtain

$$|S_2(z,\infty)| \leq 1 \Leftrightarrow \exp(x) \leq (\frac{1}{\omega^8} - 1)\frac{\exp(-x)}{(1-x)^2+y^2} + 2\frac{|1-x|+|y|}{(1-x)^2+y^2} \tag{37}$$

we could estimate for $x < 0$ *and* $y \in \mathbb{R}$ $\frac{|1-x|+|y|}{(1-x)^2+y^2} \leq 3/2$ *and* $\frac{1}{2\tan^2(\alpha)} < \frac{\exp(-x)}{(1-x)^2+y^2}$ *where* $\tan(\alpha) = y/x$.
Finally, we get the bound $\omega \leq \left(\frac{1}{8\tan^2(\alpha)+1}\right)^{1/8}$.

6 Domain Decomposition methods : Schwarz wave form relaxation methods

In this section we shall present the necessary conditions for the convergence of the overlapping Schwarz wave form relaxation method for the solution of the convection-reaction diffusion equation with constant coefficients. We will utilize the convergence analysis for the solution of the decoupled and coupled system of convection reaction diffusion equation to elaborate the impact of the coupling on the convergence of the overlapping Schwarz wave form relaxation.

6.1 Overlapping Schwarz wave form relaxation for the scalar convection reaction diffusion equation

We consider the convection diffusion reaction equation, given by

$$u_t = Du_{xx} - \nu u_x - \lambda u \ , \tag{38}$$

defined on the domain $\Omega = [0, L]$ for $T = [T_0, T_f]$, with the following initial and boundary conditions

$$u(0,t) = f_1(t), \quad u(L,t) = f_2(t), \quad u(x,T_0) = u_0 \ .$$

To solve the model problem using overlapping Schwarz wave form relaxation method, we subdivide the domain Ω in two overlapping sub-domains $\Omega_1 = [0, L_2]$ and $\Omega_2 = [L_1, L]$, where $L_1 < L_2$ and $\Omega_1 \bigcap \Omega_2 = [L_1, L_2]$ is the overlapping region for Ω_1 and Ω_2.

To start the wave form relaxation algorithm we firstly consider the solution of the model problem (38) over Ω_1 and Ω_2 as follows

$$\begin{aligned} v_t \quad &= Dv_{xx} - \nu v_x - \lambda v \text{ over } \Omega_2 \ , \quad t \in [T_0, T_f] \\ v(0,t) \quad &= f_1(t) \ , \quad t \in [T_0, T_f] \\ v(L_2,t) \ &= w(L_2,t) \ , \quad t \in [T_0, T_f] \\ v(x,T_0) &= u_0 \quad x \in \Omega_1, \end{aligned} \tag{39}$$

$$\begin{aligned} w_t \quad &= Dw_{xx} - \nu w_x - \lambda w \text{ over } \Omega_2 \ , \quad t \in [T_0, T_f] \\ w(L_1,t) \ &= v(L_1,t) \ , \quad t \in [T_0, T_f] \\ w(L,t) \quad &= f_2(t) \ , \quad t \in [T_0, T_f] \\ w(x,T_0) &= u_0 \quad x \in \Omega_2, \end{aligned} \tag{40}$$

where $v(x,t) = u(x,t)|_{\Omega_1}$ and $w(x,t) = u(x,t)|_{\Omega_2}$.

Then the Schwarz wave form relaxation is given by

$$\begin{aligned} v_t^{k+1} \quad &= Dv_{xx}^{k+1} - \nu v_x^{k+1} - \lambda v^{k+1} \text{ over } \Omega_1 \ , \quad t \in [T_0, T_f] \\ v^{k+1}(0,t) \quad &= f_1(t) \ , \quad t \in [T_0, T_f] \\ v^{k+1}(L_2,t) \ &= w^k(L_2,t) \ , \quad t \in [T_0, T_f] \\ v^{k+1}(x,T_0) &= u_0 \quad x \in \Omega_1, \end{aligned} \tag{41}$$

$$
\begin{aligned}
w_t^{k+1} &= Dw_{xx}^{k+1} - \nu w_x^{k+1} - \lambda w^{k+1} \text{ over } \Omega_2\ , \quad t \in [T_0, T_f] \\
w^{k+1}(L_1, t) &= v^k(L_1, t)\ , \quad t \in [T_0, T_f] \\
w^{k+1}(L, t) &= f_2(t)\ , \quad t \in [T_0, T_f] \\
w^{k+1}(x, T_0) &= u_0 \quad x \in \Omega_2.
\end{aligned} \tag{42}
$$

We are interested in estimating the decay of the error of the solution over the overlapping subdomains by the overlapping Schwarz wave form relaxation method over long time interval.

Let us assume that $e^{k+1}(x,t) = u(x,t) - v^{k+1}(x,t)$ and $d^{k+1}(x,t) = u(x,t) - w^{k+1}(x,t)$ is the error of (41) and (42) over Ω_1 and Ω_2 respectively. The corresponding differential equations satisfied $e^{k+1}(x,t)$ and $d^{k+1}(x,t)$ are given by

$$
\begin{aligned}
e_t^{k+1} &= De_{xx}^{k+1} - \nu e_x^{k+1} - \lambda e^{k+1} \text{ over } \Omega_1\ , \quad t \in [T_0, T_f] \\
e^{k+1}(0, t) &= 0\ , \quad t \in [T_0, T_f] \\
e^{k+1}(L_2, t) &= d^k(L_2, t)\ , \quad t \in [T_0, T_f] \\
e^{k+1}(x, T_0) &= 0 \quad x \in \Omega_1,
\end{aligned} \tag{43}
$$

$$
\begin{aligned}
d_t^{k+1} &= Dd_{xx}^{k+1} - \nu d_x^{k+1} - \lambda d^{k+1} \text{ over } \Omega_2\ , \quad t \in [T_0, T_f] \\
d^{k+1}(L_1, t) &= e^k(L_1, t)\ , \quad t \in [T_0, T_f] \\
d^{k+1}(L, t) &= 0\ , \quad t \in [T_0, T_f] \\
d^{k+1}(x, T_0) &= 0\ , \quad x \in \Omega_2.
\end{aligned} \tag{44}
$$

Defining for bounded functions $h(x,t) : \Omega \times [T_0, T] \to \mathbf{R}$ the norm

$$
||h(.,.)||_\infty := \sup_{x \in \Omega, t \in [T_0, T_f]} |h(x,t)|.
$$

The theory behind our error-estimates are based on the positivity lemma by Pao (or the maximum principle theorem), see Pao [28], that is introduced as

Lemma 11 *Let $u \in C(\overline{\Omega}_T) \cap C^{1,2}(\Omega_T)$, where $\Omega_T = \Omega \times (0, T]$ and $\partial\Omega_T = \partial\Omega \times (0, T]$, be such that*

$$
u_t - D\ u_{xx} + \nu\ u_x + c\ u \geq 0\ ,\ in\ \Omega_T \tag{45}
$$

$$
\alpha_0\ \partial u \partial\nu + \beta_0\ u \geq 0\ ,\ on\ \partial\Omega_T \tag{46}
$$

$$
u(x, 0) \geq 0\ ,\ in\ \Omega \tag{47}
$$

where $\alpha_0 \geq 0$, $\beta_0 \geq 0$, $\alpha_0 + \beta_0 > 0$ *on* $\partial\Omega_T$, *and* $c \equiv c(x,t)$ *is a bounded function in* Ω_T, *Then* $u(x,t) \geq 0$ *in* Ω_T

The convergence and error-estimates of e^{k+1} and d^{k+1} given by (43) and (44) respectively, are presented by the following theorem

Theorem 12 *Let* e^{k+1} *and* d^{k+1} *be the error from the solution of the sub-problems (39) and (40) by Schwarz wave form relaxation over* Ω_1 *and* Ω_2, *respectively, then*

$$||e^{k+2}(L_1,t)||_\infty \leq \gamma ||e^k(L_1,t)||_\infty \ ,$$

and

$$||d^{k+2}(L_2,t)||_\infty \leq \gamma ||d^k(L_1,t)||_\infty \ ,$$

where

$$\gamma = \frac{\sinh(\beta L_1)}{\sinh(\beta L_2)} \frac{\sinh(\beta(L_2 - L)}{\sinh(\beta(L_1 - L))} < 1 \ ,$$

with $\beta = \frac{\sqrt{\nu^2 + 4D\lambda}}{2D}$.

Proof 13 *For the error* e^{k+1} *and* d^{k+1}, *consider the following differential equations defined by* $\hat{e}^{k+1}$ *and* $\hat{d}^{k+1}$ *given by*

$$\begin{aligned}
\hat{e}_t^{k+1} &= D\hat{e}_{xx}^{k+1} - \nu\hat{e}_x^{k+1} - \lambda\hat{e}^{k+1} \text{ over } \Omega_1 \ , \quad t \in [T_0, T_f] \\
\hat{e}^{k+1}(0,t) &= 0 \ , \quad t \in [T_0, T_f] \\
\hat{e}^{k+1}(L_2,t) &= ||d^k(L_2,t)||_\infty \ , \quad t \in [T_0, T_f] \\
\hat{e}^{k+1}(x,T_0) &= e^{(x-L_2)\alpha} \tfrac{\sinh(\beta x)}{\sinh(\beta L_2)} ||d^k(L_2,t)||_\infty \ , \quad x \in \Omega_1
\end{aligned} \tag{48}$$

and

$$\begin{aligned}
\hat{d}_t^{k+1} &= D\hat{d}_{xx}^{k+1} - \nu\hat{d}_x^{k+1} - \lambda\hat{d}^{k+1} \text{ over } \Omega_2 \ , \quad t \in [T_0, T_f] \\
\hat{d}^{k+1}(L_1,t) &= ||e^k(L_1,t)||_\infty \ , \quad t \in [T_0, T_f] \\
\hat{d}^{k+1}(L,t) &= 0 \ , \quad t \in [T_0, T_f] \\
\hat{d}^{k+1}(x,T_0) &= e^{(x-L_1)\alpha} \tfrac{\sinh\beta(x-L)}{\sinh\beta(L_1-L)} ||e^k(L_1,t)||_\infty \ , \quad x \in \Omega_2
\end{aligned} \tag{49}$$

where $\alpha = \frac{\nu}{2D}$ *and* $\beta = \frac{\sqrt{\nu^2 + 4D\lambda}}{2D}$.

The solution to (48) and (49) is the steady state solution given by

$$\hat{e}^{k+1}(x) = e^{(x-L_2)\alpha}\frac{\sinh(\beta x)}{\sinh(\beta L_2)}||d^k(L_2,t)||_\infty \ ,$$

and

$$\hat{d}^{k+1}(x) = e^{(x-L_1)\alpha}\frac{\sinh\beta(x-L)}{\sinh\beta(L_1-L)}||e^k(L_1,t)||_\infty \ ,$$

respectively.

Hence, define $E(x,t) = \hat{e}^{k+1} - e^{k+1}$ *therefore*

$$\begin{aligned} E_t - DE_{xx} + \nu E_x + \lambda E &\geq 0 \ , \text{ over } \Omega_1 \ , \quad t \in [T_0, T_f] \\ E(0,t) &= 0 \ , \quad t \in [T_0, T_f] \\ E(L_2,t) &\geq 0 \ , \quad t \in [T_0, T_f] \\ E(x,T_0) &\geq 0 \ , \quad x \in \Omega_1 \end{aligned} \tag{50}$$

satisfies the Lemma 11 therefore

$$E(x,t) \geq 0$$

i.e.

$$|e^{k+1}| \leq \hat{e}^{k+1} \ ,$$

for all (x,t) *and similarly we conclude that*

$$|d^{k+1}| \leq \hat{d}^{k+1} \ ,$$

for all (x,t).

Then

$$|e^{k+1}(x,t)| \leq e^{(x-L_2)\alpha}\frac{\sinh(\beta x)}{\sinh(\beta L_2)}||d^k(L_2,t)||_\infty \ , \tag{51}$$

and

$$|d^{k+1}(x,t)| \leq e^{(x-L_1)\alpha}\frac{\sinh\beta(x-L_1)}{\sinh\beta(L_1-L)}||e^k(L_1,t)||_\infty \ , \tag{52}$$

Evaluate $d^k(x,t)$ *at* L_2

$$|d^k(L_2,t)| \leq \frac{\sinh\beta(L_2-L)}{\sinh\beta(L_1-L)}||e^{k-1}(L_1,t)||_\infty \ , \tag{53}$$

and substitute in (51) concluding that

$$|e^{k+1}(x,t)| \leq e^{(x-L_2)\alpha}\frac{\sinh(\beta x)}{\sinh(\beta L_2)}e^{(L_2-L_1)\alpha}\frac{\sinh\beta(L_2-L)}{\sinh\beta(L_1-L)}||e^{k-1}(L_1,t)||_\infty \ ,$$

therefore

$$|e^{k+1}(L_1,t)| \leq e^{(L_1-L_2)\alpha}\frac{\sinh(\beta L_1)}{\sinh(\beta L_2)}e^{(L_2-L_1)\alpha}\frac{\sinh\beta(L_2-L)}{\sinh\beta(L_1-L)}||e^{k-1}(L_1,t)||_\infty \ ,$$

i.e.

$$|e^{k+2}(L_1,t)| \leq \frac{\sinh(\beta L_1)}{\sinh(\beta L_2)}\frac{\sinh\beta(L_2-L)}{\sinh\beta(L_1-L)}||e^{k}(L_1,t)||_\infty \ .$$

Similarly for $d^{k+1}(x,t)$ *we conclude that*

$$|d^{k+2}(L_2,t)| \leq \frac{\sinh(\beta L_1)}{\sinh(\beta L_2)}\frac{\sinh\beta(L_2-L)}{\sinh\beta(L_1-L)}||d^{k}(L_1,t)||_\infty \ .$$

Theorem 12 shows that the convergence of of the overlapping Schwarz method depend on $\gamma = \frac{\sinh(\beta L_1)}{\sinh(\beta L_2)}\frac{\sinh\beta(L_2-L)}{\sinh\beta(L_1-L)}$. Due to the characteristic of the sinh function we will have sharp decay of the error for any $L_1 < L_2$, and also for large size of overlapping.

7 Numerical Results

7.1 Test-example : Convection-reaction equation for the simulation of the gas-mixture

We apply the operator-splitting methods for the conmvection-reaction equation.

We deal with a first order partial differential-equation given as a transport equation in the following:

$$\partial_t u_1 = -v_1\partial_x u_1 - \lambda u_1 \ , \tag{54}$$
$$\partial_t u_2 = -v_2\partial_x u_2 + \lambda u_1 \ , \tag{55}$$
$$u_1(x,0) = 1 \ , \text{for } 0.1 \leq x \leq 0.3 \ , \tag{56}$$
$$u_1(x,0) = 0 \ , \text{otherwise} \ ,$$
$$u_2(x,0) = 0 \ , \text{for } x \in [0,X] \ , \tag{57}$$

where $\lambda \in \mathbb{R}^+$ and $v_1, v_2 \in \mathbb{R}^+$. We have the time-interval $t \in [0, T]$ and the space-interval $x \in [0, X]$.

We rewrite the equation-system (54)–(57) in operator notation, and end up with the following equations :

$$\partial_t u = Au + Bu \ , \tag{58}$$
$$u(x,0) = (1,0)^T \ , \text{for } 0.1 \leq x \leq 0.3 \ , \tag{59}$$
$$u(x,0) = (0,0)^T \ , \text{otherwise} \ , \tag{60}$$

where $u = (u_1, u_2)^T$.

Our splitted operators are

$$A = \begin{pmatrix} -v_1 \partial_x & 0 \\ 0 & -v_2 \partial_x \end{pmatrix} \ , \ B = \begin{pmatrix} -\lambda & 0 \\ \lambda & 0 \end{pmatrix} \ . \tag{61}$$

We use the finite difference method as spatial discretization method and solve the time-discretization analytically.

The spatial discretization is done as follows, we concentrate on the interval $x \in [0, 1.5]$ and we consider a uniform partition of it with step $\Delta x = 0.1$. For the transport-term we use an upwind finite difference discretization given as :

$$\partial_x u_i = \frac{u_i - u_{i-1}}{\Delta x} \ . \tag{62}$$

We use for the initial-values the given impulses :

$$u_1(x) = \begin{cases} 1 & , \ 0.1 \leq x \leq 0.3 \\ 0 & , \ \text{otherwise} \end{cases} \ . \tag{63}$$

and

$$u_2(x) = 0 \ , \ x \in [0, 1.5] \tag{64}$$

For the iterative operator-splitting method and the application to our transport-equation we deal for the discretised equation with two indices. The index i is for the spatial discretization and the index j is for the iteration-steps.

We first solve all the equations with the index i, that means all 16 equations for each point. Then we do our iterative steps and we have the first time-step.

We are finished for 1 time-partition and we repeat this 4 times more for the computations of 5 partitions etc.

In the following equations we write the iterative operator splitting algorithm by taking into account the discretization in space. The time-discretization is solved analytically. On the time interval $[t^n, t^{n+1}]$ we solve the following problems consecutively for $j = 1, 3, 5, \ldots$. The split approximation at the time level $t = t^{n+1}$ is defined as $u_i^{n+1} \equiv u_{i,iter}(t^{n+1})$.

We have the following algorithm :

$$\partial_t u_{1,i,j} = -v_1/\Delta x(u_{1,i,j} - u_{1,i-1,j}) - \lambda u_{1,i,j-1} \ , \tag{65}$$
$$\partial_t u_{2,i,j} = -v_2/\Delta x(u_{2,i,j} - u_{2,i-1,j}) + \lambda u_{1,i,j-1} \ , \tag{66}$$
$$\partial_t u_{1,i,j+1} = -v_1/\Delta x(u_{1,i,j} - u_{1,i-1,j}) - \lambda u_{1,i,j+1} \ , \tag{67}$$
$$\partial_t u_{2,i,j+1} = -v_2/\Delta x(u_{2,i,j} - u_{2,i-1,j}) + \lambda u_{1,i,j+1} \ , \tag{68}$$
$$u_{1,i,j}(0) = 1 \ , \text{for } i = 1, 2, 3, \tag{69}$$
$$u_{1,i,j}(0) = 0 \ , \text{otherwise}, \tag{70}$$
$$u_{2,i,j}(0) = 0 \ , \text{for } i = 0, \ldots, 15 \ , \tag{71}$$

where $\lambda = 0.5$ and $v_1 = 0.5$ and $v_2 = 1.0$. For the time-interval we use $t \in [0, 1]$.

The analytical solution of the equation-system (54)–(57) is

$$u_1(x,t) = \begin{cases} \exp(-\lambda t) & , \text{for } 0.1 + v_1 t \leq x \leq 0.3 + v_1 t \ , \\ 0 & , \text{otherwise} \end{cases}$$

and

$$u_2(x,t) = \lambda(L_{1,2} + L_{2,2} + M_{12,2})$$

$$L_{1,2} = \begin{cases} -\frac{1}{\lambda}\exp(-\lambda t) & , \text{for } 0.1 + v_1 t \leq x \leq 0.3 + v_1 t \ , \\ 0 & , \text{otherwise} \end{cases}$$

$$L_{2,2} = \begin{cases} \frac{1}{\lambda} & , \text{for } 0.1 + v_2 t \leq x \leq 0.3 + v_2 t \ , \\ 0 & , \text{otherwise} \end{cases}$$

$$M_{12,2} = \begin{cases} \frac{1}{\lambda}\exp(-\lambda t) & \text{, for } 0.1 + v_1 t \leq x \leq 0.1 + v_2 t \ , \\ -\frac{1}{\lambda}\exp(-\lambda t)\exp(-(\frac{\lambda}{v_1 - v_2})(x - v_1 t - 0.3)) & \text{, for } 0.3 + v_1 t \leq x \leq 0.3 + v_2 t \ , \\ 0 & \text{, otherwise} \end{cases}$$

So, for the end-time $t_{end} = 1$, we check the results for the end-point $x_1 = v_1 t + 0.3$. We get the exact solution of our equation:

$$u_1(x_1, t_{end}) = 0.60653 \ , \ u_2(x_1, t_{end}) = 0$$

For the steps j and $j+1$, which are now actually ODE's, we can derive analytical solutions and apply them to our numerical scheme. The analytical solutions are given as

$$\begin{aligned} u_{1,i,j} &= u_{1,i-1,j} - \frac{\lambda \Delta x}{v_1} u_{1,i,j-1} + c_{2,i}\exp(-v_1 t/\Delta x) \\ u_{2,i,j} &= u_{2,i-1,j} + \frac{\lambda \Delta x}{v_1} u_{1,i,j-1} + c_{1,i}\exp(-v_2 t/\Delta x), \end{aligned}$$

and

$$\begin{aligned} u_{1,i,j+1} &= \frac{v_1}{\lambda \Delta x}(u_{1,i-1,j} - u_{1,i,j}) + d_{2,i}\exp(-\lambda t) \\ u_{2,i,j+1} &= \frac{v_2}{\Delta x}(u_{2,i-1,j} - u_{2,i,j})t + \frac{v_1}{\Delta x}(u_{1,i-1,j} - u_{1,i,j})t - d_{2,i}\exp(-\lambda t) + d_{1,i}, \end{aligned}$$

where $c_{1,i},\ c_{2,i},\ d_{1,i},\ d_{2,i}$ are constants depending on i and they can be computed from the initial values for $t = 0$ (as it was done in the ODE example). For $t = 0$, we get from the above four equations:

$$\begin{aligned} c_{2,i} &= u_{1,i,j}(0) - u_{1,i-1,j}(0) + \frac{\lambda \Delta x}{v_1} u_{1,i,j-1}(0) \\ c_{1,i} &= u_{2,i,j}(0) - u_{2,i-1,j}(0) - \frac{\lambda \Delta x}{v_2} u_{1,i,j-1}(0) \\ d_{2,i} &= u_{1,i,j+1}(0) - \frac{v_1}{\lambda \Delta x}(u_{1,i,j-1}(0) - u_{1,i,j}(0)) \\ d_{1,i} &= u_{2,i,j+1}(0) + d_{2,i} \end{aligned}$$

We implemented this algorithm on the computer but it didn't lead to satisfying results, as the appearing error could not reach values less than of order 10^{-1}, no matter how many time partitions or iterations we had. So we were led to use another algorithm for the expression of the analytical solutions in steps j and $j+1$.

For the time-integration we apply implicit Euler methods for the semi-discretized equations (65)-(71).

We have the following full-discretization :

$$
\begin{aligned}
u_{1,i,j}(t^{n+1}) &= (1+\frac{\tau\ v_1}{\Delta x})^{-1}(u_{1,i,j}(t^n)+\frac{\tau v_1}{\Delta x}\ u_{1,i-1,j}(t^{n+1})-\tau\ \lambda u_{1,i,j-1}(t^{n+1}))\ ,\\
u_{2,i,j}(t^{n+1}) &= (1+\frac{\tau\ v_2}{\Delta x})^{-1}(u_{2,i,j}(t^n)+\frac{\tau v_2}{\Delta x}\ u_{2,i-1,j}(t^{n+1})+\tau\ \lambda u_{1,i,j-1}(t^{n+1}))\ ,\\
u_{1,i,j+1}(t^{n+1}) &= (1+\tau\lambda)^{-1}(u_{1,i,j+1}(t^n)-\frac{\tau v_1}{\Delta x}(u_{1,i,j}(t^{n+1})-u_{1,i-1,j}(t^{n+1})))\ ,\\
u_{2,i,j+1}(t^{n+1}) &= u_{2,i,j+1}(t^n)-\frac{\tau v_2}{\Delta x}(u_{2,i,j}(t^{n+1})-u_{2,i-1,j}(t^{n+1}))+\tau\lambda u_{1,i,j+1}(t^{n+1})\ ,
\end{aligned}
$$

$j=1,3,5,\ldots,\ \tau=t^{n+1}-t^n$.
$u_{1,i,0}(t^{n+1})=1$, for $i=1,2,3$,
$u_{1,i,0}(t^{n+1})=0$, else,
$u_{2,i,0}(t^{n+1})=0$, for $i=0,\ldots,15$,
$u_{1,i,j}(0)=0$,
$u_{2,i,j}(0)=0$,
$u_{1,-1,j}(0)=0$,
$u_{2,-1,j}(0)=0$,

In order to implement the algorithm on the computer, we tried to work similarly to the ODE example. In the implementation of the ODE example we used in our computer program a vector a, in which we stored for every time partition the values of all the appearing u_1^i during the iterations. Similarly, vector b was used for u_2^i. Precisely, vector a was $[u_{10}\ \ u_1^{-1}(0)\ \ u_1^0\ \ u_1^1\ \ u_1^2\ldots u_1^{iter}]$, where the first two coordinates are the initial values, which for our example were 1 and 0 respectively, and the rest of the coordinates are the solutions calculated during all the iterations. (total number of iterations=iter)

Now, in the case of a PDE we have two dimensions, so it makes sense to use a matrix A instead of a vector. Supposing we have a total number of iterations = iter and since we have 16 points in our spatial partition, the matrix A will be of the following form:

$$A = \left[\begin{array}{c|cccc} & & & & \\ * & u_{1,0,0}(t^{n+1}) & u_{1,1,0}(t^{n+1}) & \dots & u_{1,15,0}(t^{n+1}) \\ \hline * & u_{1,0,1}(t^{n}) & u_{1,1,1}(t^{n}) & \dots & u_{1,15,1}(t^{n}) \\ u_{1,-1,1}(t^{n+1}) & u_{1,0,1}(t^{n+1}) & u_{1,1,1}(t^{n+1}) & \dots & u_{1,15,1}(t^{n+1}) \\ * & u_{1,0,2}(t^{n}) & u_{1,1,2}(t^{n}) & \dots & u_{1,15,2}(t^{n}) \\ u_{1,-1,2}(t^{n+1}) & u_{1,0,2}(t^{n+1}) & u_{1,1,2}(t^{n+1}) & \dots & u_{1,15,2}(t^{n+1}) \\ \vdots & \vdots & & & \\ * & u_{1,0,iter}(t^{n}) & u_{1,1,iter}(t^{n}) & \dots & u_{1,15,iter}(t^{n}) \\ u_{1,-1,iter}(t^{n+1}) & u_{1,0,iter}(t^{n+1}) & u_{1,1,iter}(t^{n+1}) & \dots & u_{1,15,iter}(t^{n+1}) \end{array}\right],$$

where the elements $*$ do not play any role. Similarly, we construct the matrix B for u_2. The first row represents the given initial values for the 16 points of the partition (they are 0 or 1, according to x) and they correspond to the initial values u_{10} and u_{20} in the ODE example. The first column also contains initial values, which correspond to the value $u_1^{-1}(0)$ in the case of the ODE, and they are equal to 0.

In table 1 we give the errors for the exact solutions at the end-time $t = 1$ and end-point $x = v_1 t + 0.3 = 0.8$.

7.2 First example: Diffusion-equation

We consider the two-dimensional diffusion equation given by

$$-\nabla D \nabla u = f \text{ in} \Omega = [0,1]^2, \tag{72}$$
$$u = 0 \text{ on } \partial\ \Omega \tag{73}$$

We have the following domain :

We deal with the following domain, where we have the in the domain Ω_1 the diffusion-coefficient D_1, in the domain Ω_ϵ the diffusion-coefficient D_ϵ, in the domain Ω_2 the diffusion-coefficient D_2, the thickness of the small strip is ϵ.

The right hand side $f = 1$, the boundary-conditions are complete dirichlet-boundary-conditions with zero boundary. The coefficients are $D_1 = 1.0$, $D_2 =$

Number of time-partitions	Iterative Steps	err_1	err_2
1	2	2.679116×10^{-1}	2.465165×10^{-1}
1	4	1.699365×10^{-1}	3.584424×10^{-1}
1	10	2.702681×10^{-1}	5.327567×10^{-2}
1	50	6.065295×10^{-1}	6.170954×10^{-7}
1	100	6.065307×10^{-1}	7.152770×10^{-17}
5	2	2.472959×10^{0}	6.812055×10^{-1}
5	4	1.181408×10^{1}	4.757047×10^{0}
5	10	4.680711×10^{0}	1.496981×10^{0}
5	50	8.208500×10^{-2}	7.325327×10^{-25}
5	100	8.208500×10^{-2}	1.299116×10^{-70}
10	2	2.289850×10^{2}	7.246663×10^{1}
10	4	1.121958×10^{4}	4.498364×10^{3}
10	10	8.999232×10^{4}	2.819985×10^{4}
10	50	6.737947×10^{-3}	2.593585×10^{-34}
10	100	6.737947×10^{-3}	3.160841×10^{-70}
50	2	3.166645×10^{19}	1.001479×10^{19}
50	4	2.528693×10^{32}	1.013854×10^{32}
50	10	4.750741×10^{50}	1.488686×10^{50}
50	50	1.388794×10^{-11}	3.453184×10^{-66}
50	100	1.388794×10^{-11}	$2.100221 \times 10^{-144}$

Table 1
Numerical results for the second example with the iterative splitting method.

1.0 and we deal with $D_eps = 0.1, 0.01, 0.001$

The methods are based on date-parallel Multi-grid methods with local ILU-smootheers with 2 pre- and post-smoothing steps. The grid refinement is given levels $l = 3, 4, 5, 6, 7$

We start with $\Omega_1 = [0, 0.45]x[0, 1]$ and with 3 times refinement we have $h_x = 0.05625$, $h_y = 0.125$, and $\Omega_\epsilon = [0.45, 0.55]x[0, 1]$ and with 3 times refinement we have $h_x = 0.0125$ and $h_y = 0.125$.

First test-series : $\epsilon = 0.01$

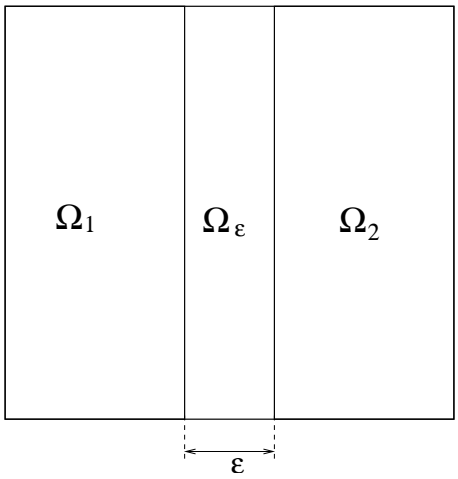

Fig. 2. The results for the Schwarz-method with 3 domains.

Coefficient D_ϵ	MG-Level	Convergence-rate
0.1	3	0.078
	4	0.073
	5	0.068
	6	0.063
	7	0.060
0.01	3	0.021
	4	0.022
	5	0.021
	6	0.019
	7	0.017
0.001	3	0.011
	4	0.015
	5	0.014
	6	0.013
	7	0.012

Table 2
The L_∞-error in time and space for the convection-diffusion-reaction-equation using FOP-method.

The graphical output for 5.

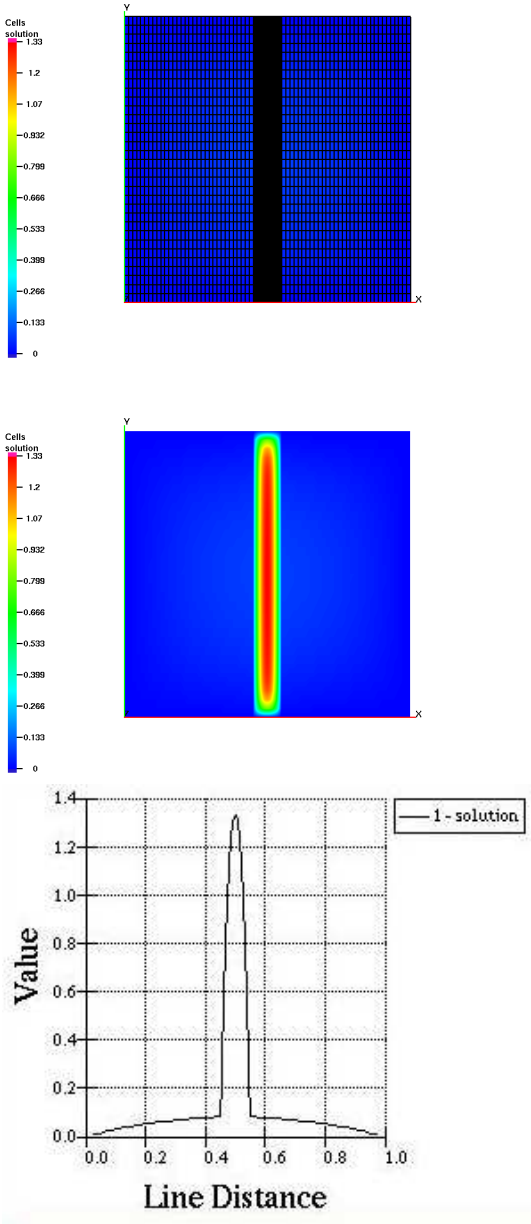

Fig. 3. The results with vertical cut and the solution in the domain for level 6 and $\epsilon = 0.1$.

7.3 Second example: Steady state Diffusion-equation with ϵ-Domains

We consider the two-dimensional diffusion equation given by

$$-\nabla D \nabla u = f \text{ in} \Omega = [0,1]^2, \tag{74}$$

$$u = 0 \text{ on } \partial\ \Omega \tag{75}$$

We have the following domain :

We deal with the following domain, where we have the in the domain Ω_1 the diffusion-coefficient D_1, in the domain Ω_ϵ the diffusion-coefficient D_ϵ, in the domain Ω_2 the diffusion-coefficient D_2, the thickness of the small strip is ϵ.

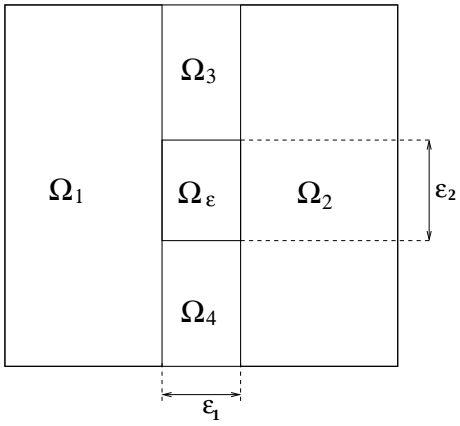

Fig. 4. The results for the Schwarz-method with 3 domains.

The right hand side $f = 1$, the boundary-conditions are complete dirichlet-boundary-conditions with zero boundary. The coefficients are $D_1 = 1.0$, $D_2 = 1.0$ and we deal with $D_epsilon = 0.1, 0.01, 0.001$

The methods are based on date-parallel Multi-grid methods with local ILU-smootheers with 2 pre- and post-smoothing steps. The grid refinement is given levels $l = 3, 4, 5, 6, 7$

We start with $\Omega_1 = [0, 0.45]x[0, 1]$ and with 3 times refinement we have $h_x = 0.05625$, $h_y = 0.125$, and $\Omega_\epsilon = [0.45, 0.55]x[0, 1]$ and with 3 times refinement we have $h_x = 0.0125$ and $h_y = 0.125$.

First test-series : $\epsilon = 0.01$

The graphical output for

7.4 Real-life problem : Crystal Growth Apparatus

We concentrate on the stationary heat conduction in potentially anisotropic materials as described in (see, e.g., **(author?)** [For01]).

We deal with the following underlying equations:

$$-\operatorname{div}(K_m(\theta)\,\nabla\,\theta) = f_m \quad \text{in } \Omega_m \qquad (m \in M), \tag{76}$$

where $\theta \geq 0$ represents absolute temperature, the symmetric and positive

Coefficient D_ϵ	MG-Level	Convergence-rate	h_{min}	maximal Anisotropy
0.1	3	0.016	0.125-2	40.0
	4	0.021	0.625-3	40.0
	5	0.036	0.313-3	40.0
	6	0.062	0.156-3	40.0
	7	0.107	0.781-4	40.0
0.01	3	0.013	0.125-2	40.0
	4	0.019	0.625-3	40.0
	5	0.035	0.313-3	40.0
	6	0.061	0.156-3	40.0
	7	0.105	0.781-4	40.0
0.001	3	0.0113	0.125-2	40.0
	4	0.020	0.625-3	40.0
	5	0.038	0.313-3	40.0
	6	0.069	0.156-3	40.0
	7	0.112	0.781-4	40.0

Table 3
Example 2, rectangular strip.

definite matrix K_m represents the thermal conductivity tensor in material m, $f_m \geq 0$ represents heat sources in material m due to some heating mechanism, e.g. induction or resistance heating, Ω_m is the domain of material m, and M is a finite index set. We consider the case where the thermal conductivity tensor is a diagonal matrix with temperature-independent anisotropy, i.e.

$$K_m(\theta) = \left(\kappa_{i,j}^m(\theta)\right), \quad \text{where} \quad \kappa_{i,j}^m(\theta) = \begin{cases} \alpha_i^m \, \kappa_{\text{iso}}^m(\theta) & \text{for } i = j, \\ 0 & \text{for } i \neq j, \end{cases} \tag{77}$$

$\kappa_{\text{iso}}^m(\theta) > 0$ being the potentially temperature-dependent thermal conductivity of the isotropic case, and $\alpha_i^m > 0$ being anisotropy coefficients. For example, the growth apparatus used in silicon carbide single crystal growth by PVT are usually insulated by graphite felt, where the fibers are aligned in one particular direction, resulting in a thermal conductivity tensor of the form (77). We apply the finite volume scheme described in section **??** and consider the anisotropy in the thermal insulation of physical vapor transport (PVT) growth apparatus in Geiser et al. [14].

The temperature θ is assumed to be continuous throughout the entire domain $\overline{\Omega}$. Continuity of the normal component of the heat flux on the interface be-

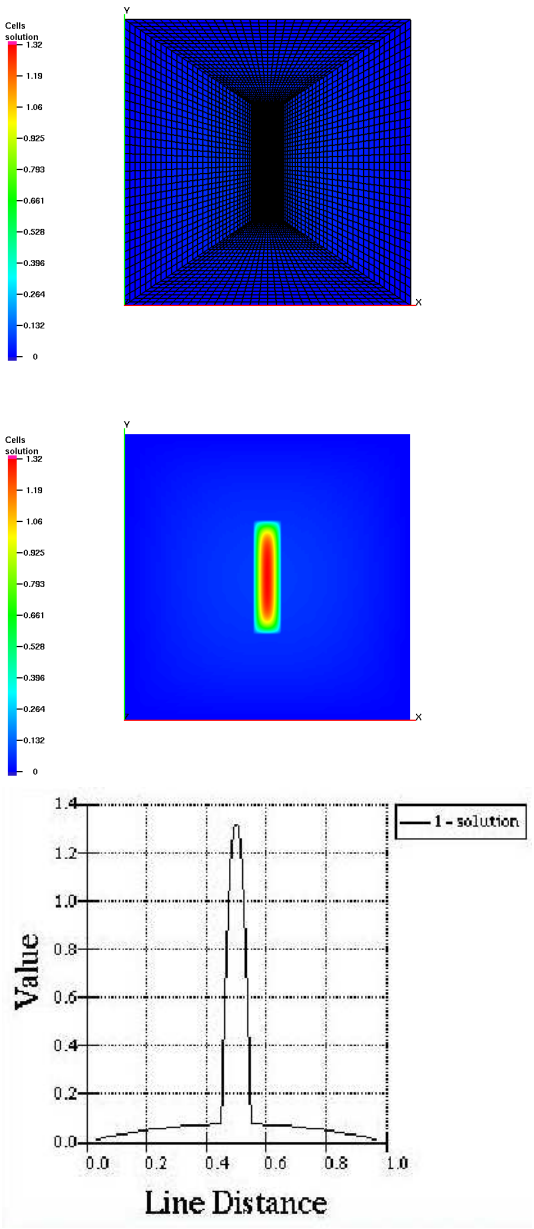

Fig. 5. The results with vertical cut and the solution in the domain for level 6 and $\epsilon = 0.1$.

tween different materials m_1 and m_2, $m_1 \neq m_2$, yields the following interface conditions, coupling the heat equations (76):

$$\left(K_{m_1}(\theta)\,\nabla\,\theta\right)\restriction_{\overline{\Omega}_{m_1}} \bullet \mathbf{n}_{m_1} = \left(K_{m_2}(\theta)\,\nabla\,\theta\right)\restriction_{\overline{\Omega}_{m_2}} \bullet \mathbf{n}_{m_1} \quad \text{on } \overline{\Omega}_{m_1} \cap \overline{\Omega}_{m_2}, \tag{78}$$

where $\restriction$ denotes restriction, and $\mathbf{n}_{m_1}$ denotes the unit normal vector pointing from material m_1 to material m_2.

We consider two types of outer boundary conditions, namely Dirichlet and

Robin conditions. To that end, we decompose $\partial\Omega$ according to (A-1):

(A-1) Let Γ_{Dir} and Γ_{Rob} be relatively open polyhedral subsets of $\partial\Omega$ such that $\partial\Omega = \overline{\Gamma}_{\mathrm{Dir}} \cup \overline{\Gamma}_{\mathrm{Rob}}$, $\Gamma_{\mathrm{Dir}} \cup \Gamma_{\mathrm{Rob}} = \emptyset$.

The boundary conditions then read

$$\theta = \theta_{\mathrm{Dir}} \text{ on } \overline{\Gamma}_{\mathrm{Dir}}, \tag{79a}$$

$$-\Big(K_m(\theta)\,\nabla\theta\Big) \bullet \mathbf{n}_m \;= \xi_m\,(\theta - \theta_{\mathrm{ext},m}) \text{ a.e. on } \Gamma_{\mathrm{Rob}} \cap \partial\Omega_m,\ m \in \mathcal{M}, \tag{79b}$$

where $\mathbf{n}_m$ is the outer unit normal to Ω_m, $\theta_{\mathrm{Dir}} \geq 0$ is the given temperature on Γ_{Dir}, $\theta_{\mathrm{ext},m} \geq 0$ is the given external temperature ambient to $\Gamma_{\mathrm{Rob}} \cap \partial\Omega_m$, and $\xi_m > 0$ is a transition coefficient.

Our apparaturs is given as follows:

The radius is 12 cm and the height is 45.3 cm. This domain represents a growth apparatus used in silicon carbide single crystal growth by the PVT method. Ω consists of six subdomains Ω_m, $m \in \{1, \ldots, 6\}$, representing the materials insulation, graphite crucible, SiC crystal seed, gas enclosure, SiC powder source, and quartz. Aiming to use realistic functions for the isotropic parts $\kappa^m_{\mathrm{iso}}(\theta)$ of the thermal conductivity tensors (cf. (77)), for gas enclosure, graphite crucible, insulation, and SiC crystal seed, we use the functions given by (A.1), (A.3b), (A.4b), and (A.7b) in Klein et al. [24]; for $\kappa^5_{\mathrm{iso}}(\theta)$ (SiC powder source), we use [22, (A.1)], and for $\kappa^6_{\mathrm{iso}}(\theta)$ (quartz), we use

$$\kappa^6_{\mathrm{iso}}(\theta) = \left(1.82 - 1.21 \cdot 10^{-3}\,\frac{\theta}{\mathrm{K}} + 1.75 \cdot 10^{-6}\,\frac{\theta^2}{\mathrm{K}^2}\right)\,\frac{\mathrm{W}}{\mathrm{m\,K}}. \tag{80}$$

Hence, all functions $\kappa^m_{\mathrm{iso}}(\theta)$ depend nonlinearly on θ. As mentioned in the Introduction, the thermal conductivity in the insulation is typically anisotropic in PVT growth apparatus. In the numerical experiments reported on below, we therefore vary the anisotropy coefficients (α^1_r, α^1_z) of the insulation while keeping $(\alpha^m_r, \alpha^m_z) = (1, 1)$ for all other materials $m \in \{2, \ldots, 5\}$.

Heat sources $f_m \neq 0$ are supposed to be present *only* in the part of Ω_2 (graphite crucible) labeled by "uniform heat sources" in the left-hand picture in Fig. 6 satisfying 5.4 cm $\leq r \leq$ 6.6 cm and 9.3 cm $\leq z \leq$ 42.0 cm. In that region, f_2 is set to the constant value $f_2 = 1.23$ MW/m^3, which corresponds to a total heating power of 1.8 kW. This serves as an approximation to the situation typically found in a radio frequency induction-heated apparatus, where a moderate skin effect concentrates the heat sources within a few millimeters of the conductor's outer surface.

Here, our main goal is to illustrate the effectiveness of our finite volume scheme to compute the temperature field in a realistic complex geometry involving ma-

terials with anisotropic thermal conductivity. If the anisotropy in the thermal conductivity of the insulation is sufficiently large, we expect the isotherms to be almost parallel to the direction with the larger anisotropy coefficient. Since using the Dirichlet boundary condition (79a) can suppress such an alignment of the isotherms, we opt to use the Robin condition (79b) on all of $\partial\Omega$ instead. For $m \in \{1, 2, 6\}$, we set $\theta_{\text{ext},m} = 500$ K and $\xi_m = 80$ W/(m^{2}K) (recall from Fig. ?? that Ω_1, Ω_2, and Ω_6 represent the insulation, the graphite crucible, and quartz, respectively, and, thus, the outer materials of the apparatus).

We now present results of numerical experiments, varying the anisotropy coefficients (α_r^1, α_z^1) in the insulation. In each case, we use a fine grid consisting of 61 222 triangles. We start with the isotropic case $(\alpha_r^1, \alpha_z^1) = (1, 1)$ depicted on the right-hand side of Fig. 6. Figure 7 shows the computed temperature fields for the moderately anisotropic cases $(\alpha_r^1, \alpha_z^1) = (10, 1)$ (left), $(\alpha_r^1, \alpha_z^1) = (1, 10)$ (middle), $(\alpha_r^1, \alpha_z^1) = (10, 1)$ in top and bottom insulation parts, $(\alpha_r^1, \alpha_z^1) = (1, 10)$ in insulation side wall (right).

The maximal temperatures established in the 7 experiments are collected in Table 4.

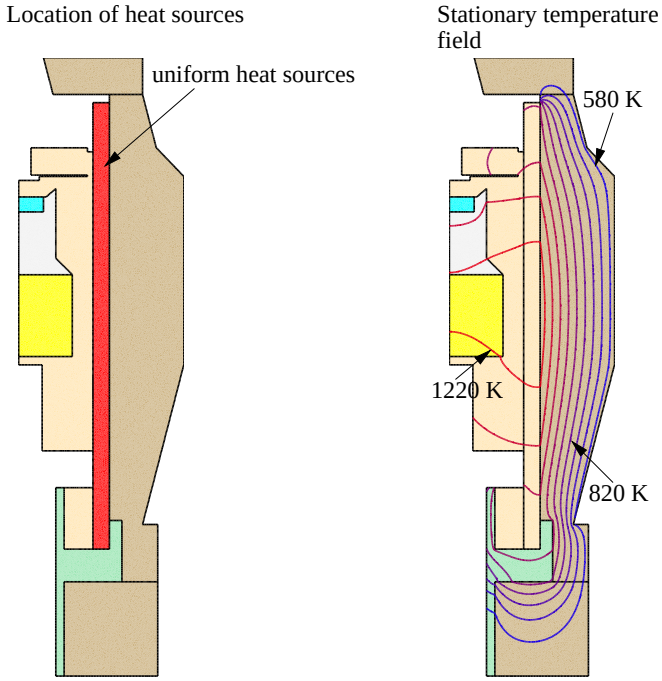

Fig. 6. Left: Location of the heat sources. Right: Computed temperature field for the isotropic case $\alpha_r^1 = \alpha_z^1 = 1$, where the isotherms are spaced at 80 K.

Comparing the temperature fields in Figures 6 - 7 as well as the maximal temperatures listed in Table 4, we find that any anisotropy reduces the effectiveness of the thermal insulation, where a stronger anisotropy results in less insulation. A stronger anisotropy results in a less effective insulation and the value above 1 improves the insulation's thermal conductivity in that direction.

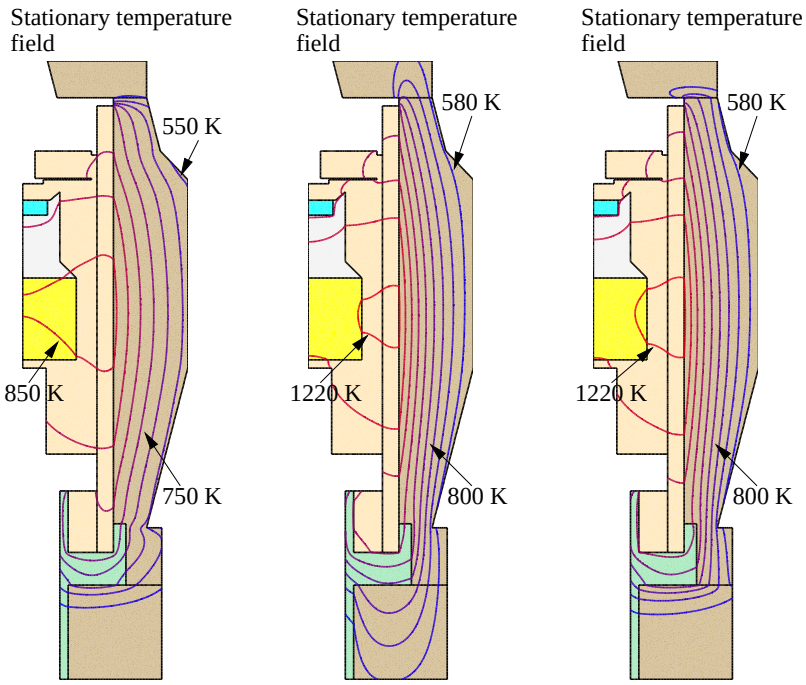

Fig. 7. Computed temperature fields for the moderately anisotropic cases $(\alpha_r^1, \alpha_z^1) = (10, 1)$ (left, isotherms spaced at 50 K); $(\alpha_r^1, \alpha_z^1) = (1, 10)$ (middle, isotherms spaced at 80 K); $(\alpha_r^1, \alpha_z^1) = (10, 1)$ in top and bottom insulation parts, $(\alpha_r^1, \alpha_z^1) = (1, 10)$ in insulation side wall (right, isotherms spaced at 80 K).

α_r^1	α_z^1	maximal temperature $[K]$
1	1	1273.18
1	10	1232.15
1-10, mixed	1-10, mixed	1238.38
10	1	918.35

Table 4
Maximal temperatures for numerical experiments, depending on the anisotropy coefficients (α_r^1, α_z^1) of the insulation (cf. Figures 6 - 7).

Similarly, when reducing one of the anisotropy coefficients to a value below 1, a stronger anisotropy would result in improved insulation.

8 Conclusion

References

[1] I. Aavatsmark, T. Barkve, Ø. Bøe, and T. Mannseth. Discretization on unstructured grids for inhomogeneous, anisotropic media. Part I: Derivation of the methods. SIAM J. Sci. Comput. **19**, No. 5, (1998), 1700–1716.

[2] I. Aavatsmark, T. Barkve, Ø. Bøe, and T. Mannseth. *Discretization on unstructured grids for inhomogeneous, anisotropic media. Part II: Discussion and numerical results.* SIAM J. Sci. Comput. **19** (1998), No. 5, 1717–1736.

[3] J. Baranger, J.F. Maitre, and F. Oudin. *Connection between finite volume and mixed finite element methods.* Math. Model. Numer. Anal. **30** (1996), No. 4, 335–465.

[4] J. Bey, *Finite-Volumen- und Mehrgitterverfahren für elliptische Randwertprobleme.* B.G. Teubner, Stuttgart, Leibzig, Germany, 1998. In German.

[5] I. Braianov and L. Volkov, *Numerical solution of a reaction-diffusion elliptic interface problem with strong anisotropy*, Computing **71** (2003), 153–173.

[6] Z. Chen, R. Li and A. Zhou. *A note on the optimal L^2-estimate of the finite volume element method.* Adv. Comput. Math. **16** (2002), 291–303.

[7] P.G. Ciarlet and J.L. Lions (eds.). *Finite Element Methods (Part 1).* Handbook of Numerical Analysis, Vol. II, North-Holland/ Elsevier, Amsterdam, The Netherlands, 1991.

[8] D. Daoud, & J. Geiser. Fractional-Splitting and Domain-Decomposition Methods for Multidimensional Parabolic Problems and Applications. Preprint No. 1096 of the Weierstrass Institute for Applied Analysis and Stochastics, Berlin, Germany, (2006).

[9] F. Dupret, P. Nicodéme, Y. Ryckmans, P. Wouters, and M.J. Crochet. *Global modelling of heat transfer in crystal growth furnaces.* Intern. J. Heat Mass Transfer **33** (1990), No. 9, 1849–1871.

[10] R. Eymard, T. Gallouët, and R. Herbin. *Finite volume methods*, pp. 713–1020 in P.G. Ciarlet and J.L. Lions (eds.). *Solution of Equations in $\mathbb{R}^n$ (Part 3); Techniques of Scientific Computing (Part 3).* Handbook of Numerical Analysis, Vol. VII, North-Holland / Elsevier, Amsterdam, The Netherlands, 2000.

[11] I. Faille, *A control volume method to solve an elliptic equation on a two-dimensional irregular mesh*, Computer Methods in Applied Meachanics and Engineering **100** (1992), pp. 275–290.

[12] I.Farago, J.Geiser. *Iterative Operator-Splitting Methods for Linear Problems*, IJCS, International Journal of Computational Sciences, Vol. 1, Nos. 1/2/3, pp. 64-74, October 2005.

[13] J. Fuhrmann, Th. Koprucki, and H. Langmach. *pdelib: An open*

modular tool box for the numerical solution of partial differential equations. Design patterns, in W. HACKBUSCH and G. WITTUM (eds.). *Proceedings of the 14th GAMM Seminar on Concepts of Numerical Software, Kiel, January 23–25, 1998*. University of Kiel, Germany, 2001.

[FL01] J. FUHRMANN and H. LANGMACH. *Stability and existence of solutions of time-implicit finite volume schemes for viscous nonlinear conservation laws*. Applied Numerical Mathematics **37** (2001), No. 1–2, 201–230.

[For01] V.F. FORMALEV. *Heat and mass transfer in anisotropic bodies*. High Temperature **39** (2001), No. 5, 753–774.

[14] J. Geiser, O. Klein, & P. Philip. Numerical simulation of heat transfer in materials with anisotropic thermal conductivity: A finite volume scheme to handle complex geometries. Preprint No. 1033, Weierstrass Institute for Applied Analysis and Stochastics, Berlin, 2005.

[15] J. Geiser. Discretisation Methods with embedded analytical solutions for convection dominated transport in porous media. Lect.Notes in Mathematics (Springer), vol.3401, (2005).

[16] J. Geiser. Discretization methods with embedded analytical solutions for convection-diffusion dispersion-reaction equations and applications. Journal of Engineering Mathematics, published, (2006).

[17] W.H. Hundsdorfer, J. Verwer W. *Numerical solution of time-dependent advection-diffusion-reaction equations*, Springer, Berlin, (2003).

[18] J.Kanney, C. Miller and C. Kelley. *Convergence of iterative split-operator approaches for approximating nonlinear reactive transport problems.* Advances in Water Resources, 26:247–261, 2003.

[19] O. Klein, P. Philip, and J. Sprekels. Modeling and simulation of sublimation growth of SiC bulk single crystals. Interfaces and Free Boundaries (6), (2004), 295–314.

[20] O. Klein, & P. Philip. Transient numerical investigation of induction heating during sublimation growth of silicon carbide single crystals. J. Crystal Growth, 247, no. 1-2, (2003), 219–235.

[21] O. KLEIN and P. PHILIP. *Correct voltage distribution for axisymmetric sinusoidal modeling of induction heating with prescribed current, voltage, or power*. IEEE Trans. Mag. **38** (2002), No. 3, 1519–1523.

[22] O. KLEIN and P. PHILIP. *Transient temperature phenomena during sublimation growth of silicon carbide single crystals*. J. Crystal Growth **249** (2003), No. 3–4, 514–522.

[23] O. KLEIN and P. PHILIP. *Transient conductive-radiative heat transfer: Discrete existence and uniqueness for a finite volume scheme*. Math. Mod. Meth. Appl. Sci. **15** (2005), No. 2, 227–258.

[24] O. KLEIN, P. PHILIP, J. SPREKELS and K. WILMAŃSKI. *Radiation- and convection-driven transient heat transfer during sublimation growth of silicon carbide single crystals*. J. Crystal Growth **222** (2001), No. 4, 832–851.

[25] D. KRÖNER. *Numerical Schemes for Conservation Laws*. Advances in Numerical Mathematics, Wiley Teubner, Chichester, UK, Stuttgart, Ger-

many, 1997.

[26] R.J. LeVeque. *Finite Volume Methods for Hyperbolic Problems*. Cambridge Texts in Applied Mathematics, Cambridge University Press, 2002.

[27] St.G. Müller, R.C. Glass, H.M. Hobgood, V.F. Tsvetkov, M. Brady, D. Henshall, D. Malta, R. Singh, J. Palmour and C.H. Carter Jr. Progress in the industrial production of SiC substrate for semiconductor devices. Mater. Sci. Eng. ,B 80 , no. 1-3, (2002), 327–331.

[28] C.V. Pao *Non Linear Parabolic and Elliptic Equation* Plenum Press, New York, 1992.

[29] M. Parashar, V. Matossian, W. Bangerth, H. Klie, B. Rutt, T.M. Kurc, U.V. Catalyuerek, J.H. Saltz, and M.F. Wheeler. Towards Dynamic Data-Driven Optimization of Oil Well Placement. International Conference on Computational Science (2) (2005), 656-663.

[30] P. Philip. Transient Numerical Simulation of Sublimation Growth of SiC Bulk Single Crystal. Modeling, Finite Volume Method, Results. Report No. 22, Weierstrass-Institute for Applied Analysis and Stochastics, Berlin, (2003).

[31] P. Philip. *Transient Numerical Simulation of Sublimation Growth of SiC Bulk Single Crystals. Modeling, Finite Volume Method, Results*. Ph.D. thesis, Department of Mathematics, Humboldt University of Berlin, Germany, 2003, Report No. 22, Weierstraß-Institut für Angewandte Analysis und Stochastik, Berlin.

[32] O. Schenk and K. Gärtner. *Solving unsymmetric sparse systems of linear equations with PARDISO*. Journal of Future Generation Computer Systems **20** (2004), No. 3, 475–487.

[33] O. Schenk, K. Gärtner, and W. Fichtner. *Scalable parallel sparse factorization with left-strategy on shared memory multiprocessor*. BIT **40** (2000), No. 1, 158–176.

[34] K. Semmelroth, N. Schulze, and G. Pensl. *Growth of SiC polytypes by the physical vapour transport technique*. J. Phys.-Condes. Matter **16** (2004), S1597–S1610.

[35] J.R. Shewchuk. *Triangle: Engineering a 2D quality mesh generator and delaunay triangulator*, in *First Workshop on Applied Computational Geometry (Philadelphia, Pennsylvania)*. ACM, May 1996, pp. 124–133.

[36] G. Strang. *On the construction and comparision of difference schemes*. SIAM J. Numer. Anal., 5:506–517, 1968.

[37] J.,G. Verwer and B. Sportisse. *A note on operator splitting in a stiff linear case*. MAS-R9830, ISSN 1386-3703, 1998.